ISSN: 0067-2904

Modulation of Chaos with Optoelectronic Feedback in Semiconductor Laser

Maha N. Adnan[1*], Kais A. Al Naimee[2]
[1]Department of Physics, College of Science, University of Baghdad, Baghdad, Iraq.
[2]Istituto Nazionale di Ottica, CNR, Largo E. Fermi 6, 50125 Firenze, Italy.

Abstract
The modulation of chaotic behavior in semiconductor laser with A.C coupling optoelectronic feedback has been numerically and experimentally reported. The experimental and numerical studying for the evaluation of chaos modulation behavior are considered in two conditions, the first condition, when the frequency of the external perturbation is varied, secondly, when the amplitude of this perturbation is changed. This dynamics of the laser output are analyzed by time series, FFT and bifurcation diagram.

Keywords: Chaos, Feedback, Modulation, Bursting

تضمين اشارات الشواش بالتغذية العكسية الكهروضوئية لليزر اشباه الموصلات

مها ناظم عدنان [1*] ، قيس عبد الستار النعيمي [2]
[1]قسم الفيزياء ، كلية العلوم، جامعة بغداد، بغداد، العراق
[2]معهد ناسيونالي، فلورنسا ، ايطالي

الخلاصة
سلوك تضمين الشواش في ليزر اشباه الموصلات ذو التغذية العكسية الكهروبصرية تم دراسته مختبريا وعدديا . الدراسات النظرية والمختبرية لتطور سلوك تضمين الشواش تحدد بشرطين ، الشرط الاول عندما يكون تردد الاضطراب الخارجي متغير ، اما الثاني عندما تكون سعة الاضطراب الخارجي متغيرة. ديناميكية الخرج الليزري تفسر باستخدام تغير اشارة الشواش مع الزمن ، تحويلات فورير والمخطط التشعب.

Introduction

The irregular oscillations for time evolutions in nonlinear dynamical systems are appeared clearly in their outputs as a deterministic manner and it's different from random processes. These oscillations are called dynamical chaos. Chaos may indicate to any state of disorder or confusion [1]. Dynamic chaos is considered as a very interesting nonlinear phenomenon which has been intensively studied during the last four decades [2]. Control of chaos, or control of chaotic systems, is the boundary field between control theory and dynamical systems theory studying when and how it is possible to control systems exhibiting irregular, chaotic behavior [3]. These phenomena can be understood in terms of a paradigmatic model known as Shilnikov Homoclinic Chaos (HC) [4]. Homoclinic chaos of the Shilnikov type, initially observed in chemical and laser [5] experiments, shows striking similarities with the electrical spike trains traveling on the axons of animal neurons [6].

*Email: maha.n.adnan@gmail.com

An important topic in neurodynamics is the bursting behavior [7] where a spiking regime is alternated by a quiescent state or subthreshold activity; in this way, the bursting shows two different time scales, the fast dynamics (spikes) and the slow one responsible for the alternation[8]. The CO_2 laser with sinusoidal modulation of the cavity losses shows a similar behavior, that is, the crisis-induced intermittency [9], For a suitable value of the modulation amplitude the system jumps between small-amplitude chaotic oscillations and an unstable periodic orbit of large amplitude[10]. The earlier observation of optical chaos in laser systems was realized by Arecchi et al. in a CO_2 laser cavity loss was modulated by an electro-optic modulator [11] and with saturable absorber. The semiconductor laser subjected to the feedback injection is suitable way to produce a chaotic dynamic. These chaotic systems using semiconductor lasers can be described by three dynamic rate equations [4] while the CO_2 laser was described by six rate equations model [12]. In order to understand these complex dynamics, frequently observed in biological environments, and to provide controllable and reproducible experiment, considerable efforts have been devoted to the search of analogous phenomena in nonlinear optical systems, and HC has been found in CO_2 laser with feedback [12, 13] and with a saturable absorber [14]. It is clear that interbursting and intrabursting periods are changed by changing the modulation frequency[15].

In this work, the experimental setup is build to study the control and modulation of chaos in a semiconductor laser with an ac-coupled optoelectronic delay feedback. The dynamics of single-mode class-B lasers (semiconductor laser), is judged by two linked variables (field density and population inversion) because the polarization term is adiabatically eliminated, evolving with two very different characteristic timescales. The application of optoelectronic feedback establishes a third degree of freedom (and a third timescale), leads to a three dimensional slow–fast system showing a chaotic oscillations as the dc-pumping current of SL and feedback strength is varied, then the generation and control of bursting achieved by a low level of perturbation signal .

Experimental work and discussions

The schematic diagram of the experimental setup is shown in Figure-1, in which it is a closed loop optical system, includes a single semiconductor laser (hp / Agilent model 8150A optical signal source) with ac-coupled optoelectronic feedback. The output laser beam is sent through an optical fiber to a photodetector, where the optical signal is converted to electrical signal. The generated electrical current is proportional to the optical intensity. Then the electrical signal is passed through a variable gain amplifier. After that, this electrical signal is fed back to the injection current of the semiconductor laser after modulated using function generator. The amplifier gain is used for determination the feedback strength. The electrical signal in narrow voltage pulses that emerged from the high pass filter is added to the laser pumping current through a mixer. The laser provides an emission with a wavelength of 850 nm and continuous output power of 2mW.

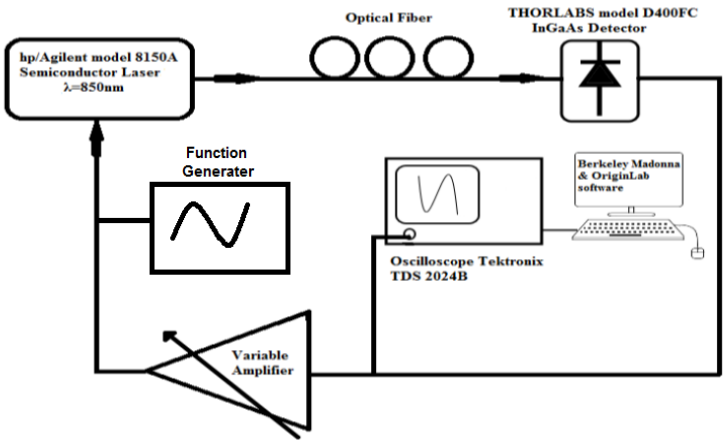

Figure 1-The sketch diagram of the experimental setup

The experimental part included the following procedure : the net amplifier gain of the entire feedback loop and the dc-pumping current have been fixed, the output signal from the amplifier modulated by external perturbation which is sinusoidal signal that has two control parameter amplitude and frequency. First we observe the dynamical sequence as demonstrated in Figure-2 that

contains the time series of different amplitude values where the frequency has been fixed at 1Hz. At low amplitude 20 mV the active phase period is equal to 0.53s, the duty cycle is 23 %, the intraburst period is 0.28s and the number of spikes in one active phase is 3 as illustrated in figure- 2(a). By gradually increasing in the amplitude of the perturbation, Figure- 2(b) shows increasing in duty cycle as a result of increasing the active phase period while the intraburst period decreases.

Additional increasing in the amplitude of perturbation shows that the duty cycle and the active phase period remain constant while intraburst period continue decreasing as shown in Figure- 2(c) Figure-3. shows the corresponding Fast Fourier Transform (FFT) (i.e. the power of each peaks frequency), where different frequencies which refer to the different peaks in time series at amplitude equal to 20, 80 and 200 mV.

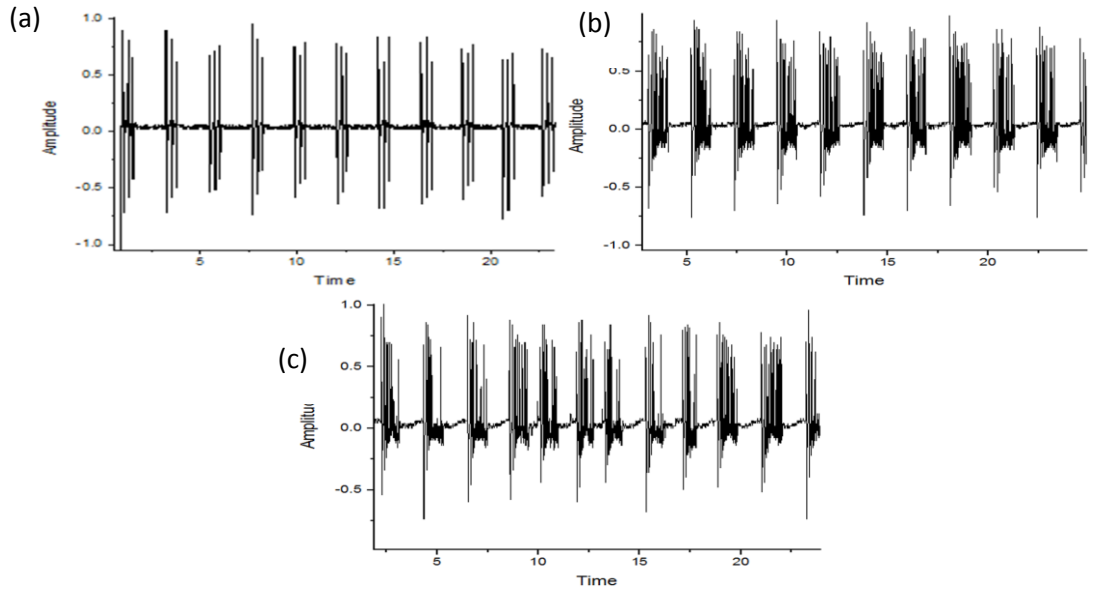

Figure 2- The experiment time series at amplitude values (a) 20mV, (b) 80mV, (c) 200mV.

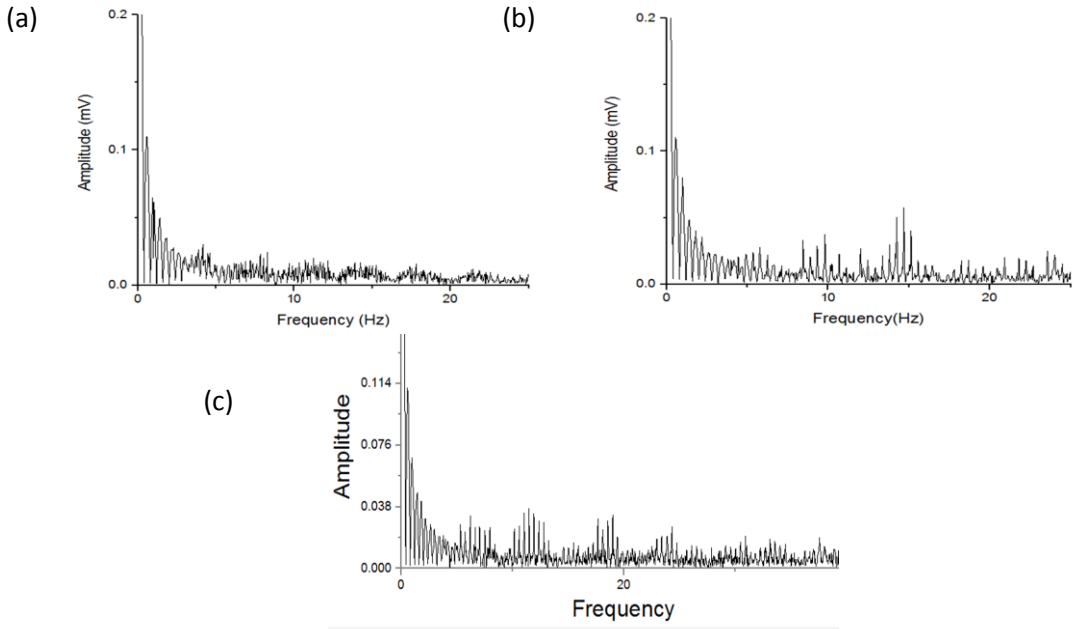

Figure 3- The Fast Fourier Transform (FFT) of the corresponding time series at amplitude values (a) 20mV, (b) 80mV, (c) 200mV.

The scenario of bursting behavior summarized by the bifurcation diagram as illustrated in Figure- 4. The bifurcation diagram exhibits the time of the laser output from peak-to-peak versus the variation of control parameter (amplitude of external perturbation) while the frequency of this perturbation is fixed. The bifurcation diagram is established within slow increase in the control parameter.

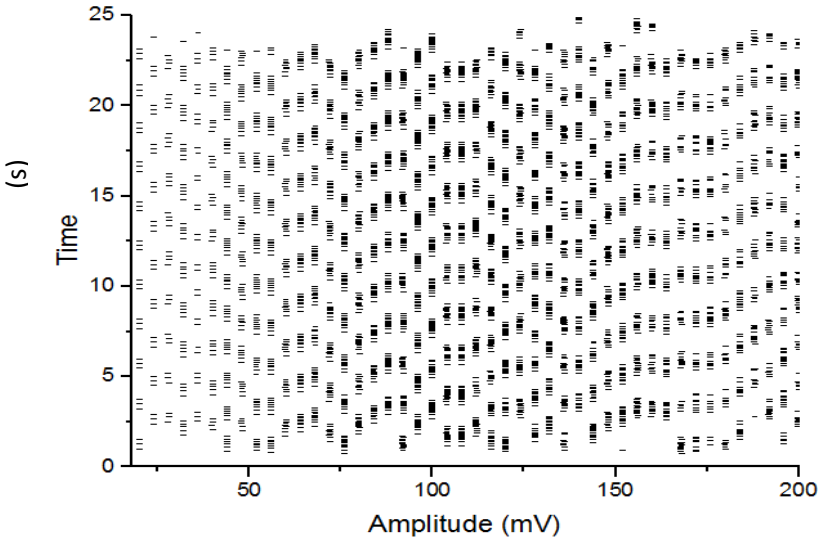

Figure 4-The bifurcation diagram obtained by the variation of amplitude of external perturbation

In Figure- 4 and Table-1, the first region from (20-80) mV the active phase period increases so that the duty cycle increases while the intraburst period is decrease and the number of spikes in one active phase period increased, by gradually increasing in the amplitude from (80- 140) mV, the duty cycle and active phase period remain constant while the intraburst period continue to decease with increasing of the number of spikes in one active phase period , then more increasing in the amplitude (140-200) mV the control of bursting is slightly missing.

Table 1-The results obtained by variation of amplitude of external perturbation

Amplitude (mV)	*active phase period (s)*	*duty cycle %*	*intraburst period*	*spikes number*
20	**0.53**	**23**	**0.28**	**3-4**
80	**1.08**	**48**	**0.21**	**12**
140	**1.06**	**48**	**0.18**	**17**
200	**1**	**45**	**0.14**	**13**

Second, when the amplitude of perturbation has been fixed at 100mV with gradually increasing in the frequency we observe the dynamical sequence as demonstrated in Figure-5 that contains the time series of different frequency values. In Figure-5(a), the sketch of the time series within this sequence is demonstrated when the frequency equal to 0.65 Hz, the active phase period is equal to 1.13 s, the duty cycle is 46 %, the intraburst period is 0.2s and the number of spikes in one active phase is 19.

In Figure-5(b) the duty cycle decreasing as a result of increasing in the active phase period and the intraburst period also decreasing at frequency equals to 1 Hz. Further increasing in the amplitude causes more decreasing in the duty cycle and the active phase period to (20% , 0.08) respectively, so that the intraburst period continue decrease as shown in Figure-5(c) that contain the time series at frequency equals to 2 Hz. Figure-6 shows the corresponding Fast Fourier Transform (FFT) (i.e. the power of each peaks frequency) at frequency equals to o.65, 1 and 2Hz.

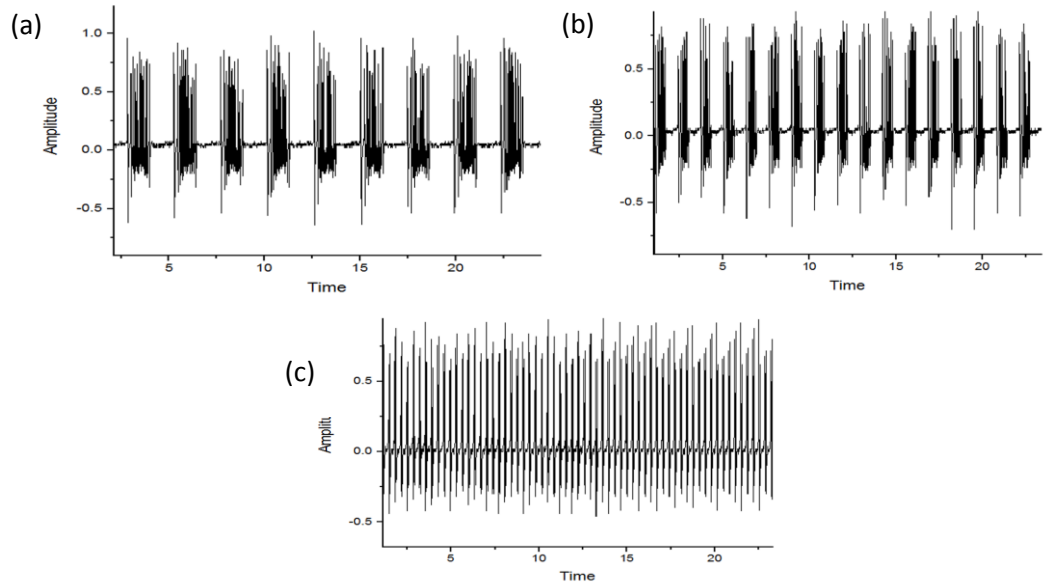

Figure 5- The experiment time series at frequency values (a) 0.65Hz, (b) 1Hz, (c) 2Hz.

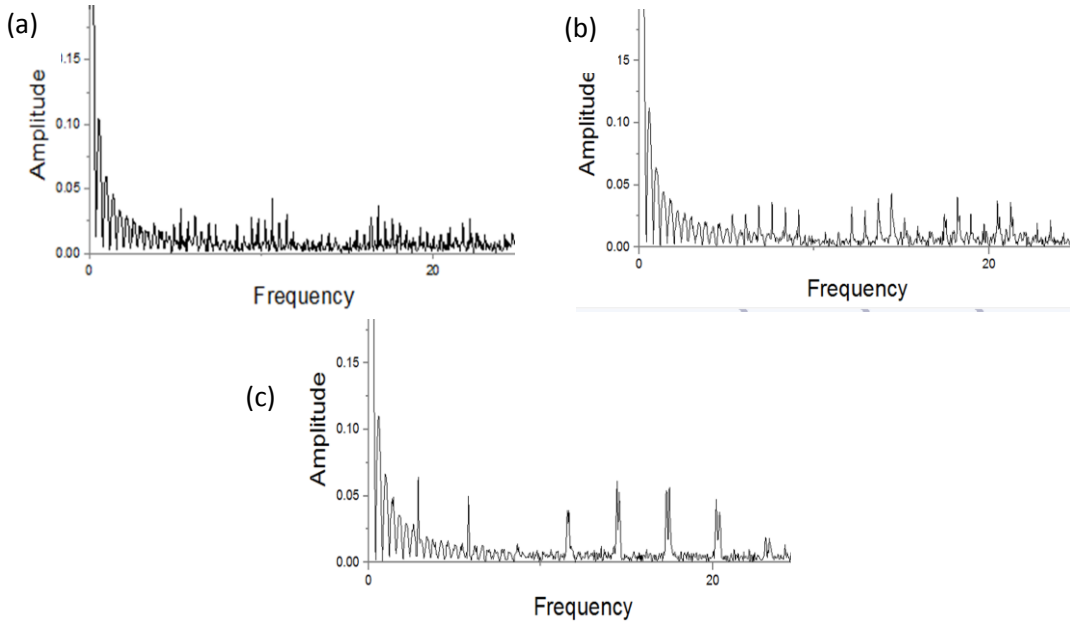

Figure 6- The Fast Fourier Transform (FFT) of the corresponding time series at (a) 0.65Hz, (b) 1Hz, (c) 2Hz.

To examine the influence of the gradually increasing in the perturbation frequency on the output dynamics of the semiconductor laser while the amplitude was kept constant, the bifurcation diagram was sketched for increment values of frequency as illustrated in Figure-7 and Table-2. In Figure-7, the first region at frequency range (0.65- 1) Hz shows decreasing in active phase period, duty cycle, intraburst period and spikes number then any more increasing in the frequency (1-2) Hz , causes decreasing in the active phase period, Therefore the two control parameter (amplitude and frequency of external perturbation) are used to display the bursting behavior.

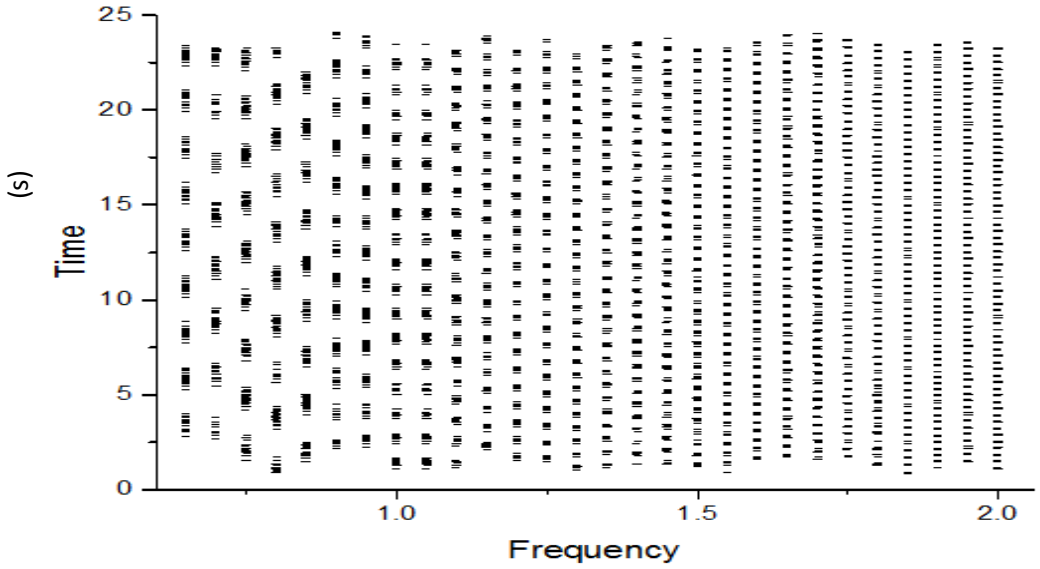

Figure 7- The bifurcation diagram obtained by the variation of frequency of external perturbation.

Table 2- The results obtained by variation of frequency of external perturbation

Frequency (Hz)	*active phase period (s)*	*duty cycle %*	*intraburst period*	*spikes number*
0.65	**1.13**	**46**	**0.2**	**19**
1	**0.58**	**43**	**0.15**	**9**
1.5	**0.16**	**29**	**0.1**	**4**
2	**0.08**	**22**	**0.07**	**2**

Dynamical model and numerical results with discussion

As previously mentioned that the field density and population inversion are two linked variables which be used to describe the complete dynamics in our system. These variables have two very different characteristics time-scales. The application of an optoelectronic feedback shows two benefits: firstly, adds a third degree of freedom in our system, secondly, adds a third much slower time-scale. The dynamics of the field density S and the population inversion N is characterized by rate equations of a single-mode semiconductor laser in which properly modified in order to include the ac-coupled optoelectronic feedback [4, 16]:

$$\dot{S} = [g\,(N - Nt) - \gamma 0]\,S \qquad (1)$$

$$\dot{N} = \{I0 + fF(I)\}/eV - \gamma c\, N - g\,(N - Nt)\,S \quad (2)$$

$$\dot{I} = -\gamma f\, I + k\,\dot{S} \quad (3)$$

Where I represents the current of high-pass filtered feedback before the nonlinear amplifier, $\boldsymbol{Io}$ is the bias current, e the electron charge, fF (I) ≡ AI/(1+s'I) is the feedback amplifier function, V is the active layer volume, Nt is the carrier density at transparency , g is the differential gain, , $\gamma 0$ is the photon damping and γc is population relaxation rate, k is a coefficient proportional to the photodetector responsivity and γf is the cutoff frequency of the high-pass filter. For analytical and numerical purposes, it is helpful to rewrite equations 1 in dimensionless form. For this purpose, we insert the new variables:

$x = (g/\gamma c)\, S$, $y = g/\gamma o\,(N\text{-}Nt)$, $w = (g/k\gamma c)\, I\text{-}x$, and the time scale $t` = \gamma ot$. where $s = \gamma c\, s'k/g$ is the saturation coefficient, $\delta 0 = (I0 - It)/(Ith - It)$ is the bais current, $f(w+x) \equiv (w+x)/(1+s(w+x))$, $Ith = eV\gamma c(\gamma 0/g + Nt)$ is the current of solitary laser, $\alpha = Ak/(eV\ \gamma o)$ is the strength of feedback, $\varepsilon = w0/\gamma o$ is the band width at resonant frequency w0, $\gamma = \gamma c / \gamma 0$. to more simplification of dimensionless equation 1,2 and 3, let $z = w+x$, therefore the above equations can be reformulated as follows:
the rate equations then become [4]

$$\dot{x} = x(y-1) \quad (4a)$$

$$\dot{y} = \gamma\left[\delta 0 - y + \alpha \frac{z}{1+sz} - xy\right] \quad (4b)$$

$$\dot{w} = -\varepsilon\,(w + x) \quad (4c)$$

where equation (4a) represents the photon density of laser source, while equation (4b) represents the population inversion of carriers and equation (4c) represents the effect of feedback. For chaos modulation, new term add to equation (4c) which is $(1+K)$ where K is an external perturbation. Then, equations (4) become:

$$\dot{x} = x(y-1) \quad (5a)$$

$$\dot{y} = \gamma\left[\delta 0 - y + \alpha \frac{z}{1+sz} - xy\right] \quad (5b)$$

$$\dot{w} = -\varepsilon\,(w + x)(1+K) \quad (5c)$$

where $K = A\sin(2\pi ft)$, A represents the amplitude of perturbation and f is the frequency. Now the theoretical results have been done by the utilizing of the fourth-order Runge-Kutta integration scheme, and apply the above equations 5(a, b and c) in Berkeley Madonna software with time step $dt = 1$. The first numerical part included the following procedure: the frequency of the perturbation has been fixed at 2.75×10^{-6} and the amplitude is gradually increased, then the model programmed with the following parameters δ0 =1.019, eps= 4×10^{-5}, α= 1, S=11 and γ= 0.01 and with initial values of parameter x1, y1 and z1 are 0.002, 1 and 0.005 respectively. At low amplitude 0.01 the active phase period is equal to 25×10^{4}, the duty cycle is 66 %, the intraburst period is 3×10^{4} and the number of spikes in one active phase is 9 as illustrated in Figure-8(a). By gradually increasing in the amplitude of the perturbation, the cycle deceases as a result of decreasing in the active phase period and the intraburst period decreases as shown in figure-8(b). Additional increasing in the amplitude shows that the duty cycle and the active phase period decreased , while intraburst period remain constant as shown in Figure-8(c). The weight of each peak frequency illustrated by the corresponding FFT in Figure-9 where many number of frequencies contributed with different amplitudes.

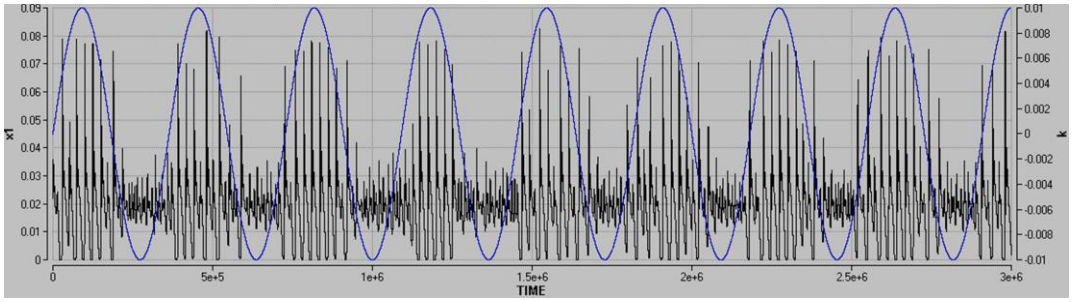

(a)

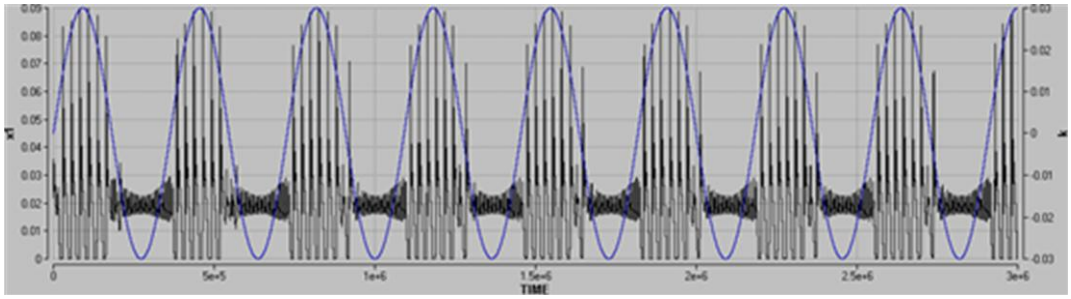

(b)

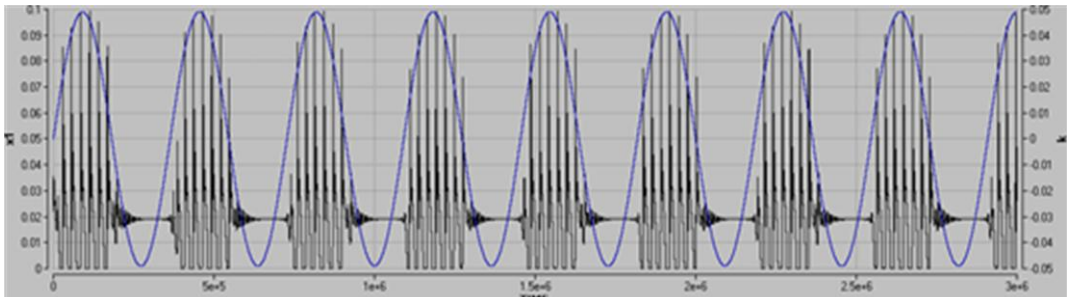

(c)

Figure 8- The numerical time series at amplitude of perturbation A (a) 0.01, (b) 0.03, (c) 0.049.

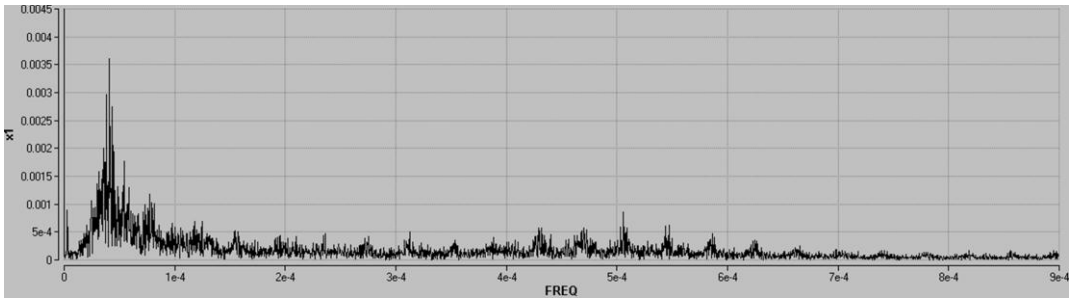

(a)

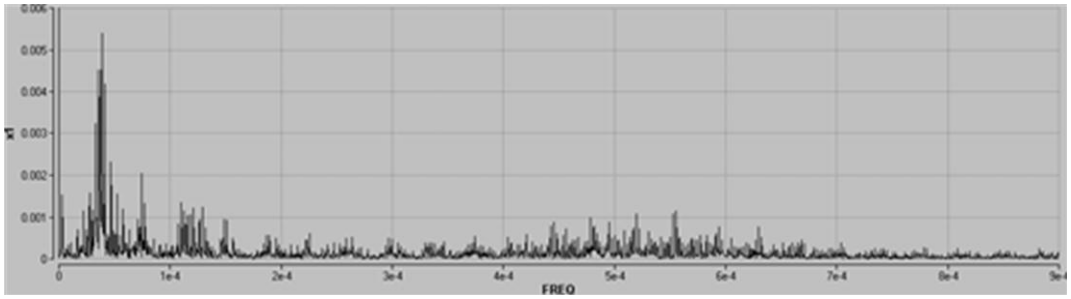

(b)

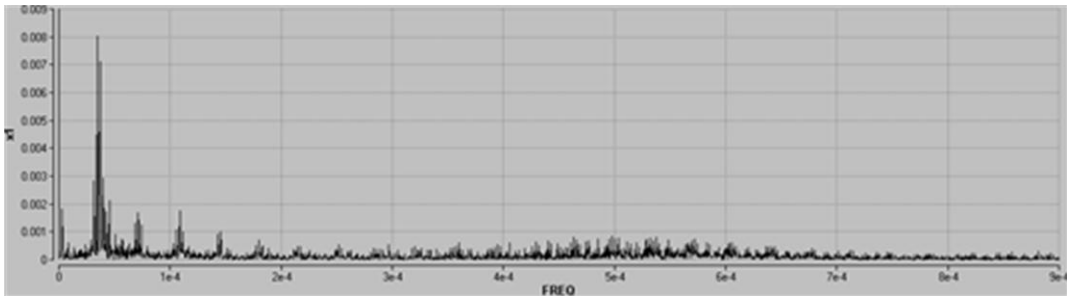

(c)

Figure 9- The Fast Fourier Transformation (FFT) of the corresponding time series at (a) 0.01, (b) 0.03, (c) 0.049,

In Figure-10 and Table-3, the first region at amplitude range (0.01- 0.02) shows decreasing in active phase period, duty cycle, intraburst period and spikes number then any more increasing in the frequency (0.02-0.049), causes decreasing in the active phase period and duty cycle, while the intraburst period remain constant.

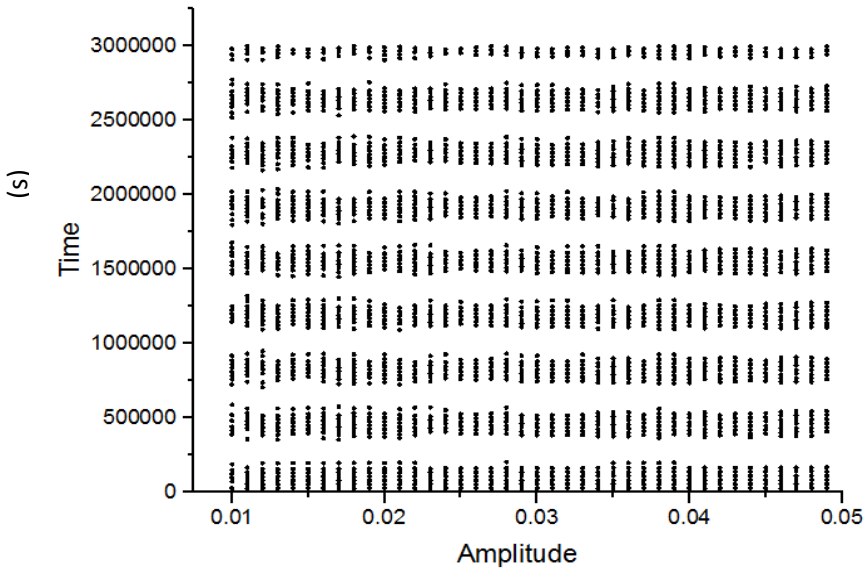

Figure 10- The numerical bifurcation diagram of the variation of perturbation amplitude A. the system parameter are f= 2.75×10^{-6}, δ0 =1.019, eps= 4×10^{-5}, α= 1, S=11 and γ= 0.01.

Table 3- The numerical results obtained by variation of amplitude of external perturbation

Amplitude	*active phase period*	*duty cycle %*	*intraburst period*	*spikes number*
0.01	**253200**	**66**	**31700**	**9**
0.02	**190000**	**51**	**26000**	**8**
0.03	**174500**	**47**	**26200**	**7**
0.04	**170000**	**46**	**27000**	**6**
0.049	**138000**	**39**	**26500**	**5**

The second numerical part included the following procedure: the amplitude of the perturbation has been fixed at 0.034 and the frequency is gradually increased, then the model programmed with the following parameters δ0 =1.019, eps= 4×10^{-5},α= 1, S=11 and γ= 0.01 and with the same initial values as before.

At perturbation frequency equals to 0.25×10^{-6} the active phase period is equal to 22×10^{6}, the duty cycle is 56 %, the intraburst period is 22×10^{3} and the number of spikes in one active phase is 27 as illustrated in Figure-11(a). By gradually increasing in the frequency perturbation, the duty cycle decreases as a result of decreasing in the active phase period and the intraburst period remain constant as shown in Figure -11(b). Additional increasing in the frequency shows that the duty cycle and the active phase period decrease, while intraburst period remain constant as shown in Figure-11(c). Figure-12 shows various heights in amplitudes and the weight of each peak frequency where many number of frequencies contributed with different frequencies.

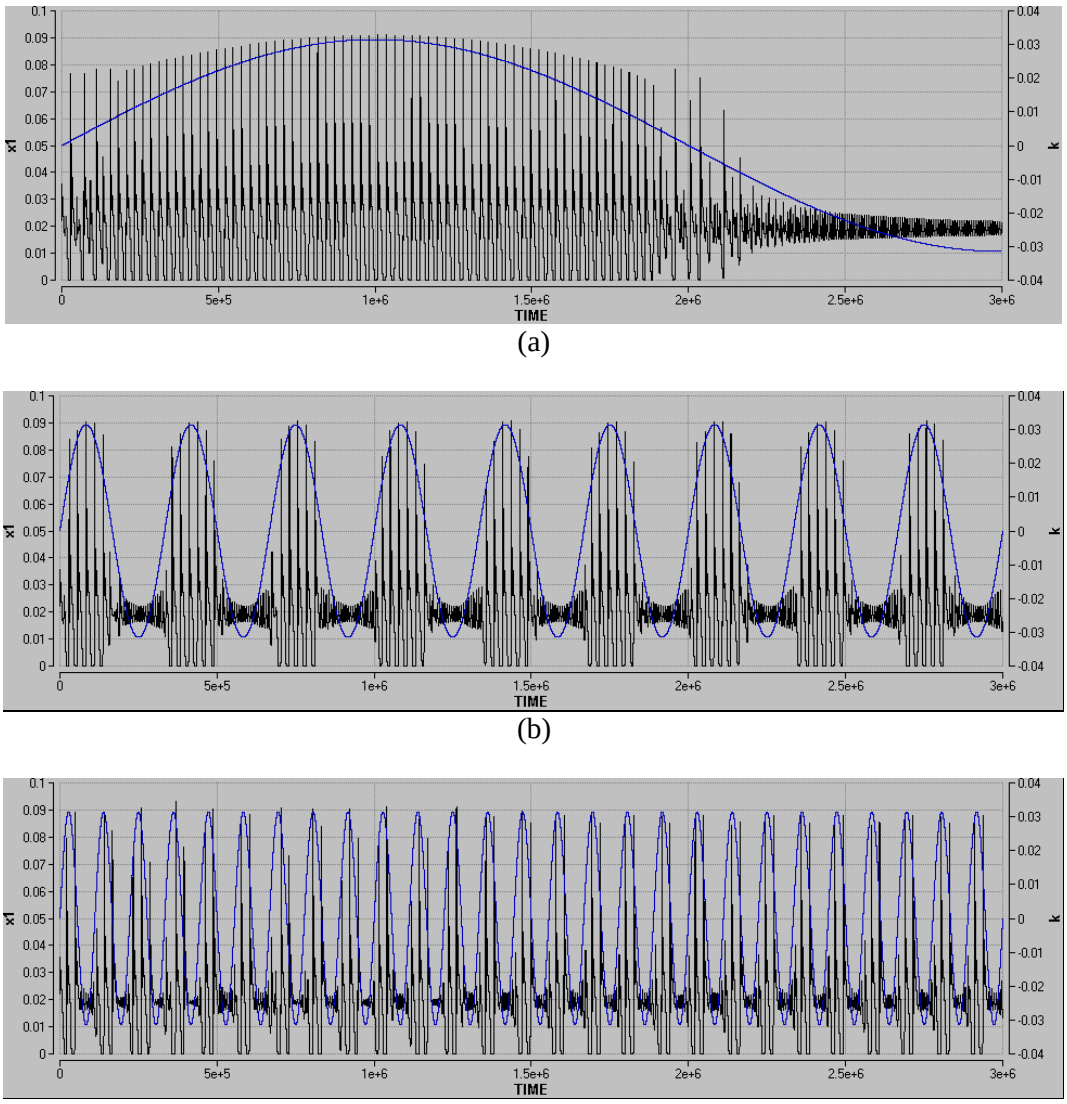

(a)

(b)

(c)

Figure 11- The numerical time series at frequency of perturbation f (a)0.25×10^{-6}, (b)3×10^{-6}, (c) 9×10^{-6}

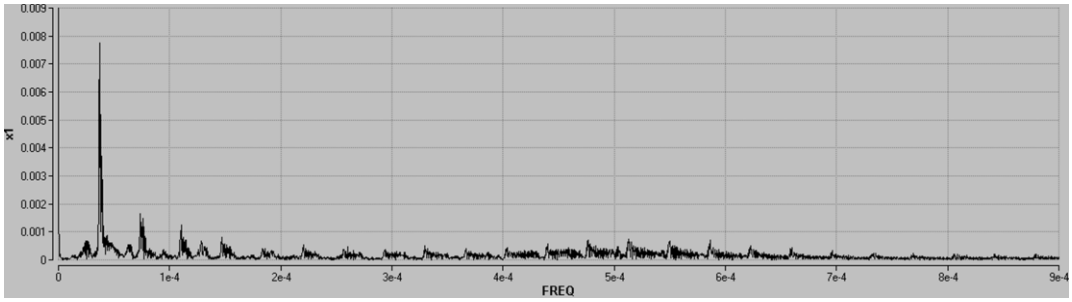

(a)

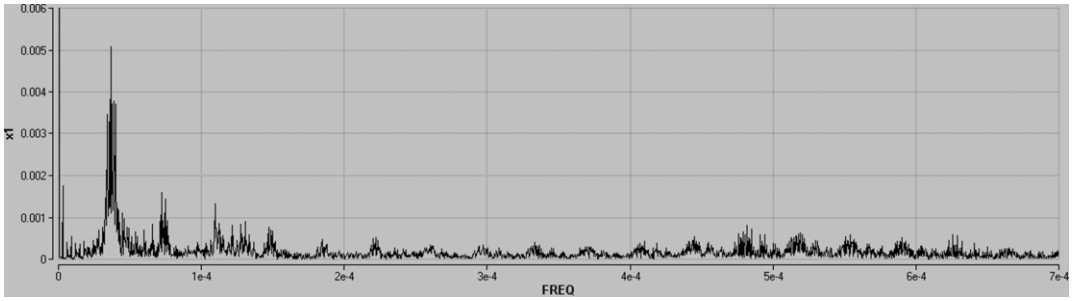

(b)

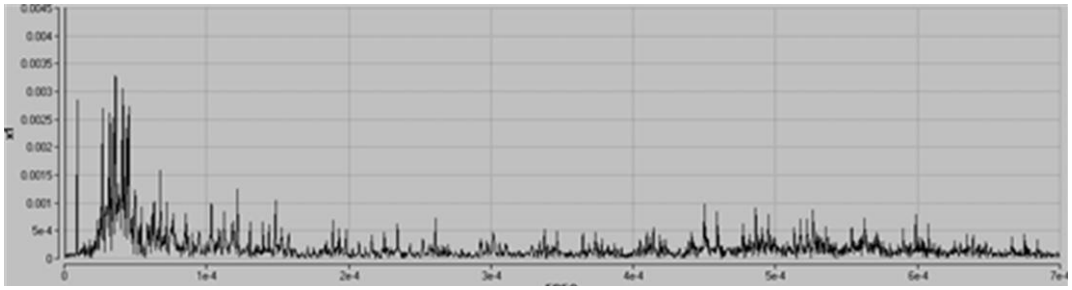

(c)

Figure 12- The Fast Fourier Transformation (FFT) of the corresponding time series at (a)0.25×10^{-6}, (b)3×10^{-6}, (c) 9×10^{-6}

The effect of frequency modulation is demonstrated in clearly manner in Figure-13 and Table-4, where the increasing of frequency causes decreasing in active phase period and duty cycle, but the intraburst period remain constant at all values of frequency.

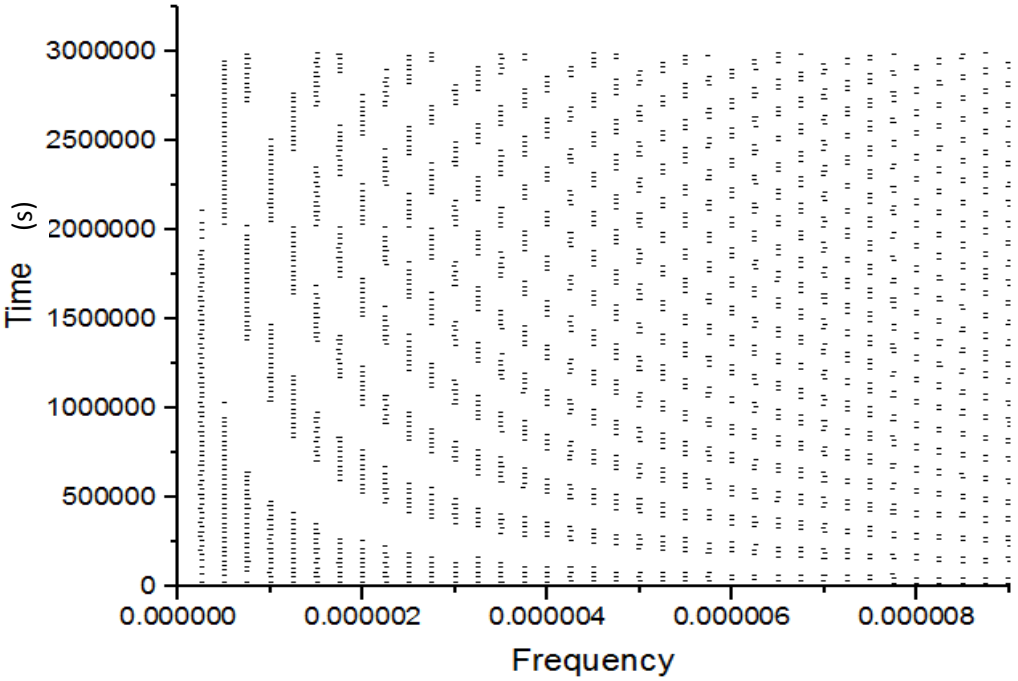

Figure 13-The numerical bifurcation diagram of the variation of perturbation frequency f. the system parameter are A=0.03, δ0 =1.019, eps= 4×10^{-5}, α= 1, S=11 and γ= 0.01.

Table 4- The numerical results obtained by variation of frequency of external perturbation

Frequency(Hz)	*active phase period*	*duty cycle %*	*intraburst period*	*spikes number*
0.25×10^{-6}	**2272500**	**56**	**26500**	**72**
3×10^{-6}	**134000**	**40**	**26000**	**6**
6×10^{-6}	**53500**	**31**	**26500**	**3**
9×10^{-6}	**22500**	**21**	**26500**	**2**

Conclusions

In conclusion, we have experimentally and numerically studied the modulation of chaos using semiconductor laser by means of optoelectronic feedback. The effect of the chaos modulation is presented showing the generation of bursting in the time series.

The control of bursting behavior can be achieved by changing in the amplitude or frequency of modulation signal, it is clear that the frequency effect on the intrabursting period, interbursting period, and duty cycle is more dominate compared to the amplitude effect.

References

1. Hilborn, R.C. **2000**. *Nonlinear dynamics: An introduction for scientists and engineers*. 2nd Ed, Oxford University Press Inc.
2. Hasan Ghassan, Kadhim A. Hubeatir A. and Kais A. Al-Naimee, **2015**. Spiking control in semiconductor laser with Ac-coupled optoelectronic feedback. *Aust. J. Basic & Appl. Sci*., 9(33), pp: 417-426.

3. Scholl E. and Schuster H. G. **2008**. *Handbook of Chaos Control*. 2nd Ed., wiley- VCH Verlag GmbH & Co. KGaA, Weinheim ISBN.

4. Al-Naimee K., Marino F., Ciszak M., Meucci R. and Arecchi T. F. **2009**. Chaotic spiking and incomplete homoclinic scenarios in semiconductor lasers with optoelectronic feedback. *New J. phys.* 11,pp: 1-13.

5. Allaria E., Arecchi T. F., Di Garbo A. and Meucci R. **2001**. Syncronization of Homoclinic chaos. *The American Physical society*, 86(5), pp: 791-794.

6. Arecchi T. F., Di Garbo A., Meucci R. and Allaria E., **2003**. Homoclinic chaos in a laser: synchronization and its implications in biological systems. *Optics and lasers in Engineering* ,39,pp: 293–304.

7. Rinzel, J. **1987**. *A formal classification of bursting mechanisms in excitable systems, in Mathematical Topics in Population Biology, Morphogenesis, and Neurosciences", eds. Teramoto, E. & Yamaguti, M.*, Lecture Notes in Biomathematics, Vol. 71, SpringerVerlag, Berlin, pp: 251–291.

8. Meucci R., Salvadori F., Ivanchenko M.V., Al-Naimee K., Zhou C., Arecchi F. T., Boccaletti S. and Kurths J. **2006**. Synchronization of spontaneous bursting in a CO_2 laser. *Physical review* E 74, 066207.

9. Meucci R., Allaria E., Salvadori F. and Arecchi T. F. **2005**. Attractor selection in choatic dynamics. *Phys. Rev. Lett*. 95, 184101.

10. Park E.H., Zaks M., and Kurths J. **1999**. Phase synchronization in the forced Lorenz system. Phys. *Rev.* E 60, pp: 6627-6638.

11. Areechi, F. T., Meucci, R. and Gadomski, W. **1987**. Laser dynamics with competing instability .*Phys. Rev. Lett.,* 58, pp: 2205-2208.

12. Pisarchik, A. N., Meucci, R. and Arecchi, F. T. **2001**. Theoretical and experimental study of discrete behavior of Shilnikov chaos in a CO_2 laser. *Eur. Phys. J.* D 13, pp: 385-391.

13. Areechi, F. T. **2005**. Feature binding as neuron Synchronization: quantum aspects. *Braz. J. Phys.*, 35, pp: 1-16.

14. Hennequin,D., Tomasi, F. D., Zambone, B. and Aremondo, E. **1998**. Homoclinic Orbit and Cycle in the instabilities of Laser with a Saturable Absorber. *phy. Rev.* A37.

15. Abdalah S.F., Al-Naimee K.A., and Meucci R. **2010**. Experimental Evidence of Slow Spiking Rate in a Semiconductor Laser by Electro-optical Feedback: Generation and Control. *Applied Physics Research,* 2(2), pp: 170-175.

16. Al-Naimee K.A., Marino F., Abdalah S.F., Ciszak M., Meucci R. and Arecchi T. F. **2010**. Excitability of periodic and choatic attractors in semiconductor lasers with optoelectronic feedback. *Eur. Phys. J.*, 58, pp: 187-189.